Journal of Power Sources 235 (2013) 251–255

Contents lists available at SciVerse ScienceDirect

Journal of Power Sources

journal homepage: www.elsevier.com/locate/jpowsour

Short communication

Lithium–oxygen cells with ionic-liquid-based electrolytes and vertically aligned carbon nanotube cathodes

Z.H. Cui, W.G. Fan, X.X. Guo*

State Key Laboratory of High Performance Ceramics and Superfine Microstructure, Shanghai Institute of Ceramics, Chinese Academy of Sciences, Shanghai 200050, PR China

HIGHLIGHTS

- Cycle performance of Li–O_2 cells with the ionic-liquid-based electrolytes was studied.
- Vertically aligned carbon nanotube cathodes facilitated clarification of reaction products.
- Abacus-ball-shaped Li_2O_2 particles produced at discharge were identified.
- Accumulation of Li carbonates around the nanotubes led to cell degradation.

ARTICLE INFO

Article history:
Received 11 November 2012
Accepted 12 February 2013
Available online 19 February 2013

Keywords:
Lithium–oxygen batteries
Ionic-liquid-based electrolytes
Vertically aligned carbon nanotubes
Lithium peroxides
Lithium carbonates

ABSTRACT

Cycle performance of Li–O_2 cells with *N*-methyl-*N*-propylpiperidinium bis(trifluoromethansulfony) imide (PP13TFSI)–$LiClO_4$ electrolytes and vertically aligned carbon nanotube (VACNT) cathodes has been investigated. It is found that both the current density and the depth of discharge have great influence on the capacity utilization, voltage polarization and cycle life. Abacus-ball-shaped Li_2O_2 particles produced at discharge are identified, and their complete decomposition at charge is confirmed. Meanwhile, formation of Li carbonates around the VACNTs is detected after the first cycle. The carbonates accumulate and gradually become predominant over Li_2O_2 upon cycling, leading to decrease of the discharge capacity and increase of the cell resistance. These results indicate that reduction of the carbonates formed around the VACNTs is of critical importance for improving cycle performance of the cells investigated here.

1. Introduction

The Li–O_2 battery with the nonaqueous electrolyte has been intensively studied recently because it may deliver a great gravimetric energy density in theory, which can achieve the target of 700 Wh kg^{-1} for the future automotive propulsion batteries [1–11]. However, as stepping forwards the application it faces many critical problems, such as limited cycle number, large voltage polarization, poor rate and cycle performance. Amongst efforts to find solutions to these problems, one of the key directions is to establish a stable nonaqueous electrolyte against superoxide radical species so that formation and decomposition of Li_2O_2 can be reversible [12–21].

Under such circumstance, carbonated-based electrolytes were studied and most of them were found to be unstable at the discharge/charge processes, forming a large amount of carbonate species [14–16]. Ether-based electrolytes such as dimethoxyethane (DME) and tetraethylene glycol dimethyl ether (TEGDME) are more stable than the carbonate-based ones against the superoxide radical species, leading to production of Li_2O_2 at the discharge as confirmed by many groups [6,9,18,20]. For the cells with the TEGDME electrolyte, Jung et al. announced achievement of 100 cycles without obvious capacity degradation [9], although Freunberger et al. stated that the capacity decreases with increasing cycle number owing to the remarkable decomposition of the electrolyte [20]. Recently, dimethyl sulfoxide (DMSO)-based electrolytes show potential for reversible and high-rate Li–O_2 cells [10,19], while the lithium anodes used in such cells should be well protected due to their reactivity to DMSO. Besides the above nonaqueous electrolytes, ionic-liquid-based electrolytes have also attracted much attention [12,13,21–24]. Their properties including the low vapor pressure and flammability, high thermal and chemical stability, and wide potential window are promising for use as the electrolytes in Li–O_2 cells. Amongst the ionic-liquid electrolytes, *N*-methyl-*N*-propylpiperidinium bis(trifluoromethansulfony)imide (PP13TFSI) is suggested to be one of good candidates for use as the electrolyte solvent [12]. It could be electrochemically stable against superoxide

* Corresponding author. Tel.: +86 21 52411032; fax: +86 21 52411802.
E-mail addresses: XXGuo@mail.sic.ac.cn, xiangxin.guo@gmail.com (X.X. Guo).

0378-7753/$ – see front matter © 2013 Elsevier B.V. All rights reserved.
http://dx.doi.org/10.1016/j.jpowsour.2013.02.025

radical as well as chemically stable against Li metal. It could also lead to a low voltage hysteresis of 0.75 V, beneficial to the electrical efficiency during cycles [12,13]. Nevertheless, in the previous reports, identification of reaction products and elucidation of the key factors limiting the cyclability of the cells with PP13TFSI-based electrolytes are still lack.

Therefore, in this work, we investigate the Li–O_2 cells using the PP13TFSI–$LiClO_4$ as the electrolytes and vertically aligned carbon nanotubes (VACNTs) grown on stainless steel (SS) meshes as the cathodes. The VACNT cathodes were intentionally selected because they are self-standing without binder or catalyst materials, avoiding the complexity caused by the reaction between these materials and the electrolytes or Li_2O_2. This is helpful for clarification of the relevant cell chemistry. Moreover, the geometry of VACNT facilitates electrons, ions and gas species to transport along the nanotube direction, favorably forming oriented products. This leads to easy characterization of the product morphologies. Taking these advantages, solid-state products formed on the VACNT cathodes and their effect on cycle performance of the cells are studied.

2. Experimental

Prior to preparing the electrolytes, the ionic liquid of PP13TFSI (Kanto Chemical Corporation) in battery grade was degassed by baking at 80 °C for 72 h in vacuum. They were further dried by stirring over lithium foil in an MBraun glove box with purified Ar under conditions of the moisture as well as the oxygen content less than 0.1 ppm. The final water content of PP13TFSI solvent in the electrolyte was below 5 ppm, measured by a Metrohm 831 KF Coulometer. $LiCiO_4$ (99.99% trace metals basis, Aldrich) as the Li salt was baked under vacuum at 90 °C for 60 h. Then the electrolytes were prepared by dissolving of 0.4 M $LiCiO_4$ into the PP13TFSI with stirring at room temperature for 12 h.

The VACNT electrodes were purchased from Microphase Co. LTD in Japan, composed of VACNTs grown on SS meshes. The mass of the carbon nanotubes was approximately 2.0 mg cm^{-2} and their specific surface areas are approximately 80 m^2 g^{-1} as measured by ASAP 2010 system. Transmission electron microscope (TEM) results that provide more microstructure information are given in Fig. S1. Before cell assembly, the VACNT electrodes were dried at 80 °C under vacuum for 48 h.

Each Li–O_2 cell in Swagelok-type was assembled in an Ar-filled glove box with oxygen and moisture levels below 0.1 ppm, consisting of a lithium foil anode (0.5 mm thick), a VACNT cathode and a glass fiber (Whatman) separator soaked with the electrolyte. Then the cells were sealed in the in-house built chambers with the inlet and outlet tubes for oxygen flowing (as shown in Fig. S2), transferred into an incubator which was maintained at a constant temperature of 60 °C. With an oxygen flow of 20 sccm, the cells were firstly rested for 4 h with the stabilized open circuit voltage (OCV) of approximately 2.8 V. Then the discharge and charge measurements were conducted by a battery tester (Arbin BT2000). The electrochemical impedance spectroscopy (EIS) measurements were carried out after the cells being equilibrated till the OCV reaching the stabilized value, i.e. ~2.8 V. The EIS spectra were recorded using an electrochemical workstation (Autolab) with a frequency response analyzer in frequency range of 0.01–10^5 Hz under an ac voltage in amplitude of 5 mV.

For X-ray diffraction (XRD) measurement, the discharged or charged VACNT cathodes were taken out from the cells in the Ar-filled glove box, washed with CH_3CN and dried on a filter paper under vacuum, and mounted in the sample holder which was sealed by two silicon-glue rings together with a stainless-steel plate and a Be window, as depicted in Fig. S3. The XRD scans were carried out using a diffractometer (D8 Discover, Bruker) with Cu K_α radiation in a reflection mode. Detection of the morphology variation upon cycling was conducted by scanning electron microscope (SEM, FEI Magellan 400). Compositions on the product surfaces were characterized using X-ray photoelectron spectrometer (XPS, ESCAlab-250) with an Al anode source. For XPS measurement, Li_2O_2 and Li_2CO_3 powders pressed on Indium were used for reference samples. All the samples were pre-sputtered using 2 kV argon ions at a pressure of 3×10^{-9} Pa. For all the above measurements, the samples during transfer were carefully protected with Ar atmosphere without exposing to ambient air.

3. Results and discussion

The first discharge and charge profiles of the Li/PP13TFSI–$LiClO_4/O_2$ cells measured at the current density ranging from 0.1 to 0.3 mA cm^{-2} and in the voltage range of 2.0–4.0 V are displayed in Fig. 1. The specific capacity is calculated according to the mass of carbon in the VACNT cathodes. It can be seen that the discharge capacity is as high as ~3500 mAh g^{-1}_{VACNT} at 0.1 mA cm^{-2} even without any catalysts. Such capacity dramatically decreases with increasing current density, which retains ~1000 mAh g^{-1}_{VACNT} at 0.3 mA cm^{-2}. Meanwhile, if the potential values are extracted from the middle of the sloppy plateau as referred to Ref. [25], the voltage hysteresis values are calculated to be 0.70 V, 0.85 V and 0.89 V for the cycle profiles measured at 0.1 mA cm^{-2}, 0.2 mA cm^{-2} and 0.3 mA cm^{-2}, respectively. In addition, the initial coulombic efficiency is 79% for 0.1 mA cm^{-2}, 74% for 0.2 mA cm^{-2} and 71% for 0.3 mA cm^{-2}. Therefore, the above results clearly indicate that the increased current density leads to the decrease of the storage capacity as well as the decrease of the initial coulombic efficiency while the increase of the voltage polarization.

Fig. 2(a) shows the cycle curves for the cells tested at the current density of 0.2 mA cm^{-2}. Fig. 2(b) gives the discharge capacity as a function of cycle number. It is clear that the discharge capacity dramatically decreases with increasing cycle number. The capacity only retains 20% after 20 cycles. Simultaneously, the voltage polarization increases with increasing cycle number. Similar to Ref. [26], the cycle number can be greatly extended if the maximum discharge/charge capacities are limited to be 800 mAh g^{-1}_{VACNT} during cycles in range of 2.0–4.0 V. After 20 cycles, the discharge capacity retains 56% of that for the first discharge, as displayed in Fig. S4.

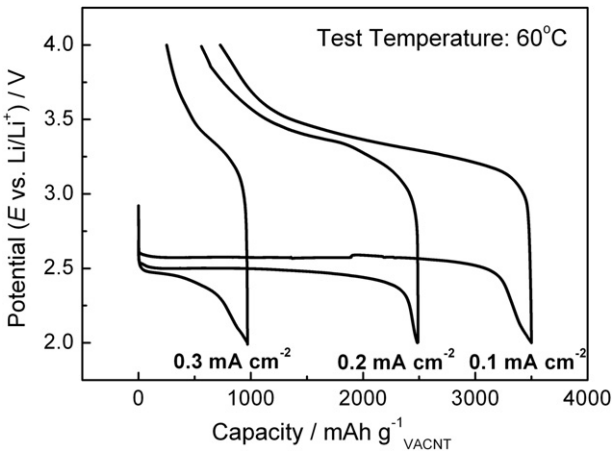

Fig. 1. The first discharge and charge profiles for the Li/PP13TFSI–$LiClO_4/O_2$ cells at the current density ranging from 0.1 to 0.3 mA cm^{-2} in the voltage range of 2.0–4.0 V. The test temperature is 60 °C. The specific capacity is calculated according to the mass of carbon in the VACNT cathodes.

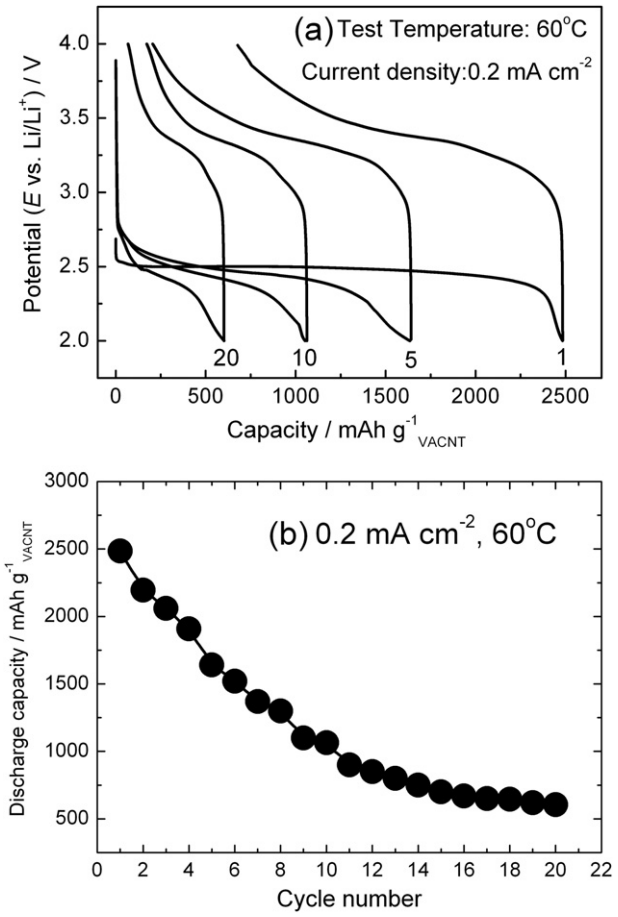

Fig. 2. (a) Cycle performance for the cells tested at the current density of 0.2 mA cm^{-2} and the voltage range of 2.0–4.0 V; (b) discharge capacity as a function of cycle number corresponding to (a).

In order to clarify the key factors limiting the cycle numbers of the cells, compositional and morphological evolutions of the VACNT cathodes at different discharge and charge stages were investigated. Fig. 3 shows the XRD curves measured on the VACNT cathodes from the cells tested at the current density of 0.2 mA cm^{-2}. It can be clearly seen that Li_2O_2 peaks appear after the first discharge and completely disappear after the first recharge. After the 5th and 8th discharges, the Li_2O_2 peaks are still visible although their intensities become smaller compared to the intensity for the first discharge. After the 21st discharge, the Li_2O_2 peaks cannot be observed, implying that the products of Li_2O_2 are negligible in this case.

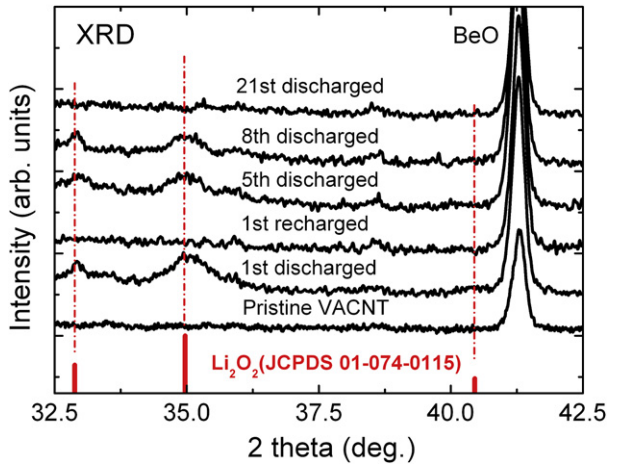

Fig. 3. XRD scans on the VACNT cathodes disassembled from the cells after the discharge and the charge in different cycles. The cells were tested at the current density of 0.2 mA cm^{-2} in the voltage range of 2.0–4.0 V. The pattern of the pristine VACNT is presented for comparison.

Fig. 4(a)–(d) show the SEM images for the VACNT cathodes at different discharge and charge stages. It is interesting that a lot of particles in shape of abacus balls are formed around the VACNT after the first discharge, as can be seen in Fig. 4(a) (especially as indicated by the arrows in the figure). Combined the above XRD and the XPS results presented in the following, these abacus-ball-shaped particles can be attributed to the Li_2O_2. They nucleate and grow around the nanotubes. Such morphology of the Li_2O_2 formed in ionic-liquid-based Li–O_2 cells is for the first time reported as far as we know. How to understand such growth model needs further investigations.

After the first recharge, the abacus-ball-shaped Li_2O_2 particles disappear, as shown in Fig. 4(b). Meanwhile, the individual nanotubes can be distinguished though some of them are still bunched. Together with the above XRD results shown in Fig. 3, it can be drawn the conclusion that the Li_2O_2 particles are formed and completely decomposed in the first discharge/charge processes here. Fig. 4(c) shows the morphology of the cathode after the 5th discharge. Compared to Fig. 4(a), the number of the abacus-ball-shaped Li_2O_2 particles obviously decreases. Some rust-like materials seem to cover the nanotubes. After the 21st discharge as shown in Fig. 4(d), no abacus-ball-shaped Li_2O_2 particles are visible. Instead, the nanotubes seem to be completely coated by the rust-like materials.

According to the XRD results for the cathode after the 21st discharge, the rust-like materials are most probably amorphous. In order to identify their composition, XPS measurement was carried out. The results are presented in Fig. 5. As can be seen in the figure, after the 1st discharge Li_2O_2 relevant peaks can be clearly observed, while the carbonate relevant ones are negligible. After the 1st recharge, the intensity of Li_2O_2 relevant peak markedly decreases, while that related to the carbonate increases. After the 21st discharge, the peak intensities of the carbonate-related peaks become predominant, as shown in both Fig. 5(a) and (b). These results clearly indicate that the Li_2O_2 is the predominant solid products after the first discharge, which is replaced by the carbonates after the 21st discharge.

Correspondingly, electrochemical impedance spectroscopy (EIS) measurement was carried out. Before each record of the spectroscopy, the cell was equilibrated till the potential reaching the OCV value before the first discharge (i.e. 2.8 V). The EIS results are displayed in Fig. 6(a) and (b). It can be seen that the semicircles gradually increase with increasing cycle number. Though it is difficult to fit the spectra by the precise equivalent circuit owing to the absence of reference electrodes [18], it is no problem to draw the conclusion that the overall cell resistance increases with cycles.

On basis of all the above results, it is reasonable to describe the reactions during cycles as follows: Li_2O_2 particles are produced by the discharge to 2.0 V, which center around the outer walls of the VACNTs. They are decomposed completely by the recharge to 4.0 V. Carbonate species as by-products accumulate with cycles, which coat the VACNT surfaces and block the electronic transfer along the cathodes. Such passivation not only suppresses the Li_2O_2 formation resulting in the decreased discharge capacity but also enlarges the voltage polarization during cycles. When the VACNT cathodes are predominantly covered by the carbonates, the cells terminate. According to the previous report [27–29], it is most probable that in the cells investigated here the carbonate species result from

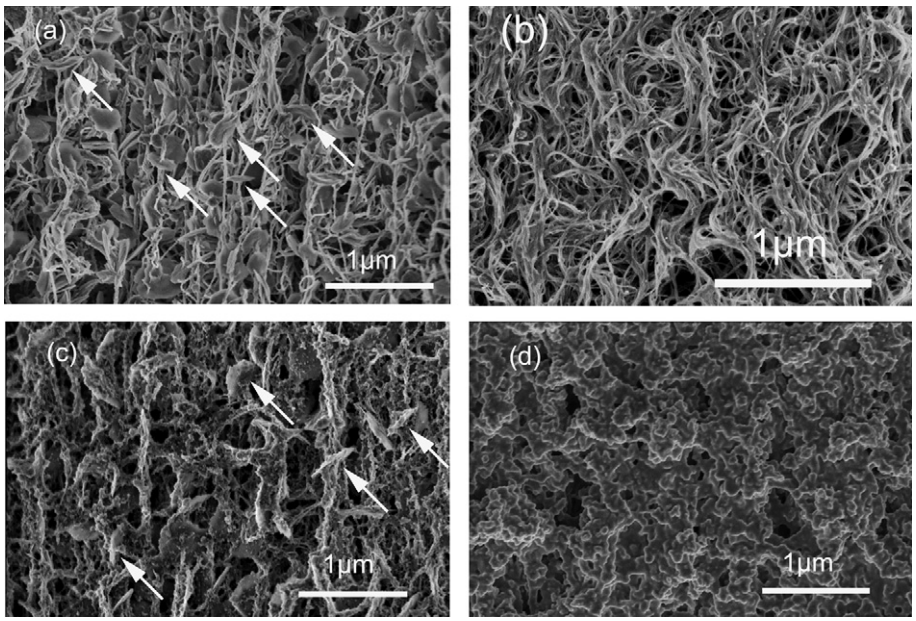

Fig. 4. SEM images for the VACNT cathodes disassembled from the cells after (a) the first discharge to 2.0 V; (b) the first recharged to 4.0 V; (c) the 5th discharge and (d) the 21st discharge at the current density of 0.2 mA cm^{-2} in the voltage range of 2.0–4.0 V.

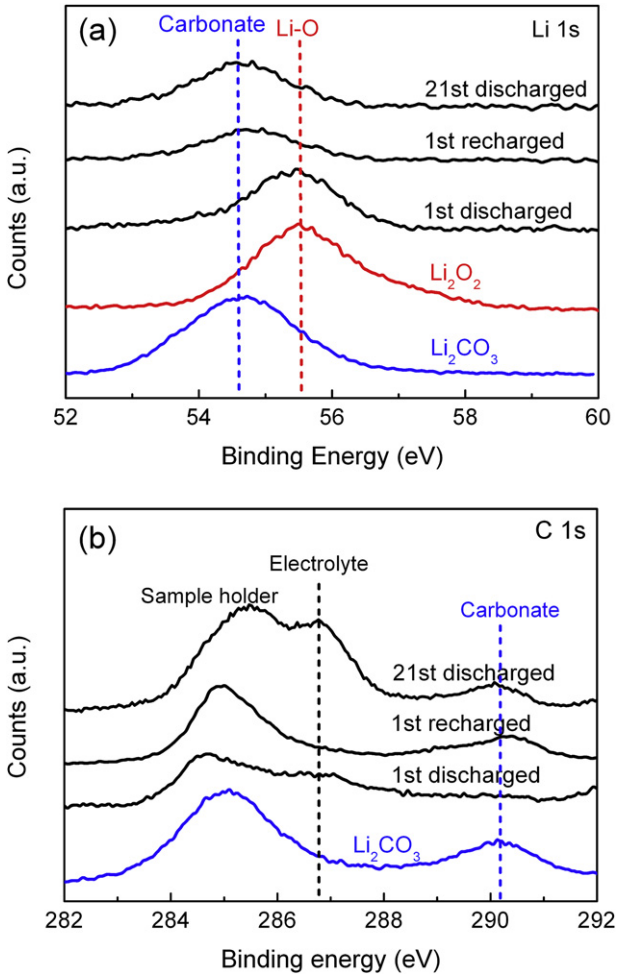

Fig. 5. XPS spectra of (a) Li 1s and (b) C 1s for the VACNT cathodes disassembled from the cells after the 1st discharge/charge and the 21st discharge processes. Li_2O_2 and Li_2CO_3 powders pressed on Indium were used for the reference samples.

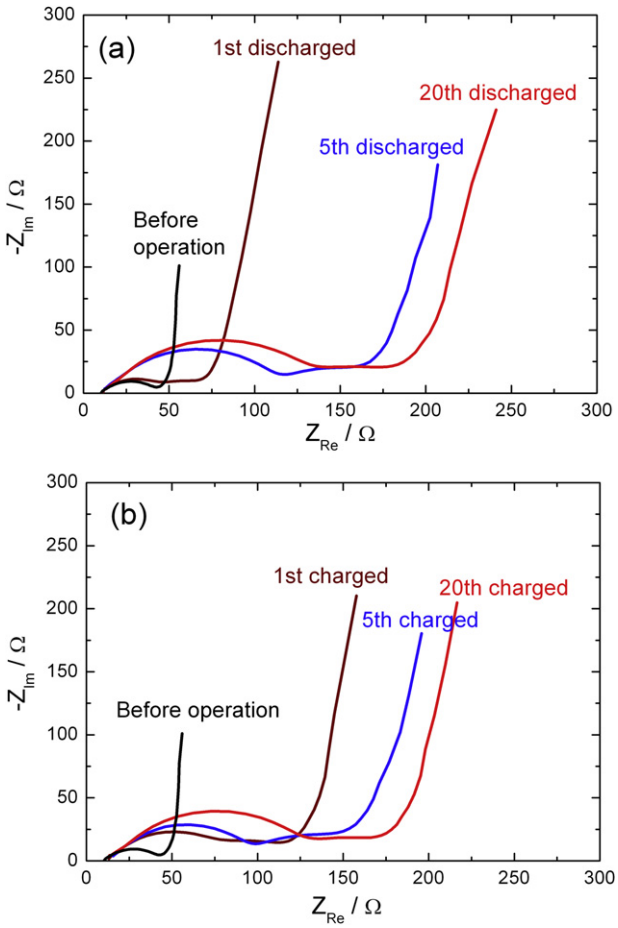

Fig. 6. Electrochemical impedance spectroscopy (EIS) profiles for the cells (a) discharged and (b) recharged at the current density of 0.2 mA cm^{-2}. The test temperatures were 60 °C. Before each measurement, the cell was equilibrated till the potential reaching the OCV value before the first discharge (i.e. 2.8 V).

reaction between the Li_2O_2 and the C cathode. Whether some carbonates also arise from the reaction between the Li_2O_2 and the ionic-liquid electrolyte needs further study.

4. Conclusions

We have studied the cycle performance of the Li–O_2 cells with the PP13TFSI–$LiClO_4$ electrolytes and the VACNT cathodes. The cycle capacity and cycle life are found to be greatly dependent on the current density as well as the depth of discharge. If in the discharge/charge processes tested at 0.2 mA cm^{-1} and in the potential range from 2.0 to 4.0 V, the discharge capacity can only retain 20% after 20 cycles. If combined with the limited maximum discharge capacity of 800 mAh g^{-1}_{VACNT}, the retention of discharge capacity can reach 56% after 20 cycles. It is demonstrated that the Li_2O_2 is produced at discharge and decomposed at charge. Morphology of abacus-ball-shaped Li_2O_2 as solid products has been observed. Upon cycling, amount of Li_2O_2 decreases while that of the Li carbonates increases. These results clearly indicate that aggregation of the carbonates around the cathodes is the main factor causing the cell degradation, which implies that reduction of carbonate formation is necessary for improvement of the cell cyclability.

Acknowledgment

This work was supported by the Key Project of the Chinese Academy of Sciences under Grant No. KGZD-EW-202-2, Sony Corporation, “Hundred Talent Program” of Chinese Academy of Sciences, and the Science Foundation for Young Researchers of State Key Laboratory of High Performance Ceramics and Superfine Microstructures (SKL201104). Dr. Yongming Li, Dr. Keisuke Shimizu, Dr. Hiroyuki Morioka, and Dr. Eishi Endo are acknowledged for helpful discussions.

Appendix A. Supplementary data

Supplementary data related to this article can be found at http://dx.doi.org/10.1016/j.jpowsour.2013.02.025.

References

[1] K.M. Abraham, Z. Jiang, J. Electrochem. Soc. 143 (1996) 1–5.
[2] P.G. Bruce, S.A. Freunberger, L.J. Hardwick, J.-M. Tarascon, Nat. Mater. 11 (2012) 19–29.
[3] G. Girishkumar, B. McCloskey, A.C. Luntz, S. Swanson, W. Wilcke, J. Phys. Chem. Lett. 652 (2010) 2193–2203.
[4] J. Christensen, P. Albertus, R.S. Sanchez-Carrera, T. Lohmann, B. Kozinsky, R. Liedtke, J. Ahmed, A. Kojic, J. Electrochem. Soc. 159 (2012) R1–R30.
[5] F.J. Li, R. Ohnishi, Y. Yamada, J. Kubota, K. Domen, A. Yamada, H.S. Zhou, Chem. Commun. 49 (2013) 1175–1177.
[6] Y.-C. Lu, D.G. Kwabi, K.P.C. Yao, J.R. Harding, J. Zhou, L. Zuin, Y. Shao-Horn, Energy Environ. Sci. 4 (2011) 2999–3007.
[7] R. Black, B. Adams, L.F. Nazar, Adv. Energy Mater. 2 (2012) 801–815.
[8] J.-G. Zhang, D.Y. Wang, W. Xu, J. Xiao, R.E. Williford, J. Power Sources 195 (2010) 4332–4337.
[9] H.-G. Jung, J. Hassoun, J.-B. Park, Y.-K. Sun, B. Scrosati, Nat. Chem. 4 (2012) 579–585.
[10] Z. Peng, S.A. Freunberger, Y. Chen, P.G. Bruce, Science 337 (2012) 563–566.
[11] S. Dong, X. Chen, K.J. Zhang, L. Gu, L.X. Zhang, X.H. Zhou, L.F. Li, Z.H. Liu, P.X. Han, H.X. Xu, J.H. Yao, C.J. Zhang, X.Y. Zhang, C.Q. Shang, G.L. Cui, L.Q. Chen, Chem. Commun. 47 (2011) 11291–11293.
[12] K. Takechi, S. Higashi, F. Mizuno, H. Nishikoori, H. Iba, T. Shiga, ECS Electrochem. Lett. 1 (2012) A27–A29.
[13] F. Mizuno, S. Nakanishi, A. Shirasawa, K. Takechi, T. Shiga, H. Nishikoori, H. Iba, Electrochemistry 79 (2011) 876–881.
[14] F. Mizuno, S. Nakanishi, Y. Kotani, S. Yokoishi, H. Iba, Electrochemistry 78 (2010) 403–405.
[15] S.A. Freunberger, Y.H. Chen, Z.Q. Peng, J.M. Griffin, L.J. Hardwick, F. Bard, P. Novak, P.G. Bruce, J. Am. Chem. Soc. 133 (2011) 8040–8047.
[16] G.M. Veith, N.J. Dudney, J. Howe, J. Nanda, J. Phys. Chem. C 115 (2011) 14325–14333.
[17] Y.H. Chen, S.A. Freunberger, Z.Q. Peng, F. Bardé, P.G. Bruce, J. Am. Chem. Soc. 134 (2012) 7952–7957.
[18] C.O. Laoire, S. Mukerjee, E.J. Plichta, M.A. Hendrickson, K.M. Abraham, J. Electrochem. Soc. 158 (2011) A302–A308.
[19] D. Xu, Z.-L. Wang, J.-J. Xu, L.-L. Zhang, X.-B. Zhang, Chem. Commun. 48 (2012) 6948–6950.
[20] S.A. Freunberger, Y.H. Chen, N.E. Drewett, L.J. Hardwick, F. Bardé, P.G. Bruce, Angew. Chem. Int. Ed. 50 (2011) 1–6.
[21] C.J. Allen, S. Mukerjee, E.J. Plichta, M.A. Hendrickson, K.M. Abraham, J. Phys. Chem. Lett. 2 (2011) 2420–2424.
[22] L. Cecchetto, M. Salomon, B. Scrosati, F. Croce, J. Power Sources 213 (2012) 233–238.
[23] H. Wang, X.-Z. Liao, L. Li, H. Chen, Q.-Z. Jiang, Y.-S. He, Z.-F. Ma, J. Electrochem. Soc. 159 (2012) A1874–A1879.
[24] F. Soavi, S. Monaco, M. Mastragostino, J. Power Sources 224 (2013) 115–119.
[25] P.L. Taberna, S. Mitra, P. Poizot, P. Simon, J.-M. Tarascon, Nat. Mater. 5 (2006) 567–573.
[26] H.-D. Lim, K.-Y. Park, H. Gwon, J. Hong, H. Kim, K. Kang, Chem. Commun. 48 (2012) 8374–8376.
[27] B.D. McCloskey, A. Speidel, R. Scheffler, D.C. Miller, V. Viswanathan, J.S. Hummelshøj, J.K. Nørskov, A.C. Luntz, J. Phys. Chem. Lett. 3 (2012) 997–1001.
[28] B.D. McCloskey, D.S. Bethune, R.M. Shelby, G. Girishkumar, A.C. Luntz, J. Phys. Chem. Lett. 2 (2011) 1161–1166.
[29] B.M. Gallant, R.R. Mitchell, D.G. Kwabi, J.G. Zhou, L. Zuin, C.V. Thompson, Y. Shao-Horn, J. Phys. Chem. C (2012). http://dx.doi.org/10.1021/jp308093b.